# Mechanical Weyl Modes in Topological Maxwell Lattices

D. Zeb Rocklin,[1,*] Bryan Gin–ge Chen,[2,†] Martin Falk,[3] Vincenzo Vitelli,[2] and T. C. Lubensky[4]
[1]Department of Physics, University of Michigan, 450 Church Street, Ann Arbor, Michigan 48109, USA
[2]Instituut-Lorentz, Universiteit Leiden, 2300 RA Leiden, The Netherlands
[3]Department of Physics, Massachusetts Institute of Technology, 77 Massachusetts Avenue, Cambridge, Massachusetts 02139-4307, USA
[4]Department of Physics and Astronomy, University of Pennsylvania, Philadelphia, Pennsylvania 19104, USA
(Received 22 October 2015; published 1 April 2016)

We show that two-dimensional mechanical lattices can generically display topologically protected bulk zero-energy phonon modes at isolated points in the Brillouin zone, analogs of massless fermion modes of Weyl semimetals. We focus on deformed square lattices as the simplest Maxwell lattices, characterized by equal numbers of constraints and degrees of freedom, with this property. The Weyl points appear at the origin of the Brillouin zone along directions with vanishing sound speed and move away to the zone edge (or return to the origin) where they annihilate. Our results suggest a design strategy for topological metamaterials with bulk low-frequency acoustic modes and elastic instabilities at a particular, tunable finite wave vector.

DOI: 10.1103/PhysRevLett.116.135503

The topological properties of the energy operator and associated functions in wave vector (momentum) space can determine important properties of physical systems [1–3]. In quantum condensed matter systems, topological invariants guarantee the existence and robustness of electronic states at free surfaces and domain walls in polyacetylene [4,5], quantum Hall systems [6,7], and topological insulators [8–13] whose bulk electronic spectra are fully gapped (i.e., conduction and valence bands separated by a gap at all wave numbers). More recently, topological phononic and photonic states have been identified in suitably engineered classical materials as well [14–33], provided that the band structure of the corresponding wavelike excitations has a nontrivial topology.

A special class of topological mechanical states occurs in Maxwell lattices, periodic structures in which the number of constraints equals the number of degrees of freedom in each unit cell [34]. In these mechanical frames, zero-energy modes and states of self-stress (SSSs) are the analogs of particles and holes in electronic topological materials [16]. A zero-energy (frequency) mode is the linearization of a mechanism, a motion of the system in which no elastic components are stretched [19,20]. States of self-stress on the other hand guide the focusing of an applied stress and can be exploited to selectively pattern buckling or failure [18]. Such mechanical states can be topologically protected in Maxwell lattices, such as the distorted kagome lattices of Ref. [16], in which no zero modes exist in the bulk phonon spectra (except those required by translational invariance at wave vector $\boldsymbol{k} = 0$). These lattices are the analog of a fully gapped electronic material. They are characterized by a topological polarization equal to a lattice vector $\boldsymbol{R}_T$ (which can be zero) that, along with a local polarization $\boldsymbol{R}_L$, determines the number of zero modes localized at free surfaces, interior domain walls separating different polarizations, and dislocations [17]. Because $\boldsymbol{R}_T$ only changes upon closing the bulk phonon gap, these modes are robust against disorder or imperfections.

In this Letter we demonstrate how to create topologically protected zero modes and states of self-stress that extend throughout a sample. These enable the topological design of bulk soft deformation and material failure in a generic class of mechanical structures. As prototypes, we study the distorted square lattices of masses and springs shown in Fig. 1, and we show that they have phases that are two-dimensional mechanical analogs of Weyl semimetals [35–39]. In the latter materials, the valence and conduction bands touch at isolated points in the Brillouin zone (BZ), with the equivalent phonon dispersion for the mechanical lattice shown in Fig. 1(a). Points at which two or four bands touch are usually called Weyl and Dirac points, respectively. These points, which are essentially wave number vortices in two dimensions and hedgehogs in three dimensions, are characterized by a winding or Chern number [1,3] and are topologically protected in that they can disappear only if points of opposite sign meet and annihilate or if symmetry-changing terms are introduced into the Hamiltonian. Weyl semimetals exhibit lines of surface states at the Fermi level that terminate at the projection of the Weyl points onto the surface BZ. Weyl points have also been predicted [40] and observed [41] in photonic crystals and certain mechanical systems with pinning constraints that gap out translations [23]. In contrast, our examples consist of ordinary spring networks, which suggests that the Weyl phenomenon is in fact generic to Maxwell lattices of sufficient complexity.

Our distorted square lattices are defined by the components of their two primitive lattice vectors and their four

 

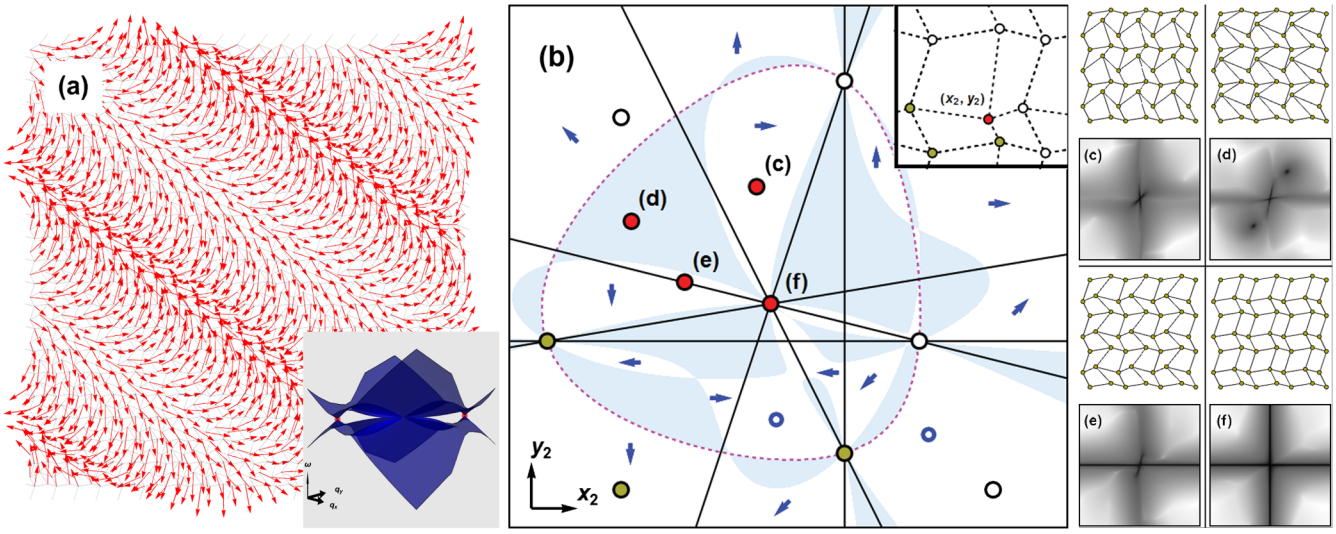


FIG. 1. (a) Deformed square lattices can have sinusoidal bulk zero modes (red arrows) corresponding to Weyl points where two bands touch in the phonon dispersion (inset). (b) The phase diagram of a deformed square lattice with the positions of three sites fixed and the position of the remaining site given by the position $(x_2, y_2)$. The inset shows the three fixed (yellow) sites, one position of the varying (red) site, and (white) sites in neighboring crystal cells. (c)–(f) Lattices (top) with phonon dispersions (bottom) with dark areas indicating low-energy modes in the Brillouin zone. In panel (b), white areas such as (c) lack Weyl points and are marked with a blue arrow indicating their topological polarization. The blue-shaded areas such as (d) correspond to Weyl lattices. Open boundaries between the white and blue regions indicate where Weyl points emerge at $\boldsymbol{k} = (0, 0)$ while the pink dashed boundary indicates where they annihilate at $\boldsymbol{k} = (\pi, \pi)$. Lattices on the special lines, such as (e), lie between topological polarizations and possess lines of zero modes along $k_{x(y)} = 0$, while at the special point (f) there are two zero modes along each of $k_{x(y)} = 0$.

basis vectors, for a twelve-dimensional full phase space. We restrict our attention to a representative two-dimensional space by varying only the components of a single basis vector, holding fixed (with dimensionless lengths) lattice vectors $\ell_1 = (1, 0)$ and $\ell_2 = (0, 1)$ and basis vectors $\mathbf{b}_1 = (0, 0)$, $\mathbf{b}_3 = (0.6, 0.1)$, and $\mathbf{b}_4 = (-0.2, 0.4)$. The resultant 2D phase diagram, shown in Fig. 1(b) exhibits a rich phenomenology: (1) a special point at the origin with two orthogonal lines of zero modes in its spectrum, (2) special lines along which the spectrum exhibits a single line of zero modes, (3) finite regions in which the spectrum is fully gapped and characterized by topological polarizations $\boldsymbol{R}_T$, and (4) finite regions whose spectrum contains Weyl points. Along paths in region (4), pairs of oppositely charged Weyl points corresponding to zero frequency bulk modes appear at the origin of the BZ along directions with quadratic, rather than linear, dispersions (discussed later in text) and move across the zone edge, annihilating either at the origin or at $\boldsymbol{k} = (\pi, \pi)$. The lattices on the low-dimensional special point and special lines are critical lattices that require fine tuning to reach. In contrast, the polarization (3) and Weyl (4) regions occupy extended two-dimensional areas in the phase diagram and do not require special fine tuning to reach. Because the Weyl modes have zero energy at nonzero wave number, lattices in region (4) have an instability that is missed by standard long-wavelength elasticity. The existence of Weyl points has significant consequences for response at the boundaries, leading to a wave number–dependent count of boundary modes and SSSs.

One can continuously change the crystal basis so as to pass from a lattice of one polarization to another either by crossing a special line or by going through a region of Weyl lattices. The latter process, which we now develop in detail, brings pairs of zero modes into and out of the bulk. In contrast, crossing through a critical lattice brings a full line of edge modes into the bulk at a particular point in parameter space.

Lattices of periodically repeated unit cells in $d$ dimensions with $n$ sites (nodes) and $n_B$ bonds per unit cell under periodic boundary conditions (PBCs) are characterized (see the Supplemental Material [42] and Refs. [34,43]) by an $n_B \times dn$ compatibility matrix $\mathbf{C}(\boldsymbol{k})$ for each wave vector $\boldsymbol{k}$ in the BZ relating the $dn$-dimensional vector $\boldsymbol{u}(\boldsymbol{k})$ of site displacements to the $n_B$-dimensional vector $\boldsymbol{e}(\boldsymbol{k})$ of bond extensions via $\mathbf{C}(\boldsymbol{k})\boldsymbol{u}(\boldsymbol{k}) = \boldsymbol{e}(\boldsymbol{k})$ and by the $dn \times n_B$ equilibrium matrix $\mathbf{Q}(\boldsymbol{k}) = \mathbf{C}^{\dagger}(\boldsymbol{k})$ relating forces $\boldsymbol{f}(\boldsymbol{k})$ to bond tensions $\boldsymbol{t}(\boldsymbol{k})$ via $\mathbf{Q}(\boldsymbol{k})\boldsymbol{t}(\boldsymbol{k}) = \boldsymbol{f}(\boldsymbol{k})$. The dynamical matrix (for systems with unit masses and spring constants) is $\mathbf{D} = \mathbf{Q}(\boldsymbol{k})\mathbf{C}(\boldsymbol{k})$. Vectors $\boldsymbol{u}(\boldsymbol{k})$ in the null space of $\mathbf{C}(\boldsymbol{k})$ do not stretch bonds and, therefore, correspond to zero modes. Vectors $\boldsymbol{t}(\boldsymbol{k})$ in the null space of $\mathbf{Q}(\boldsymbol{k})$ describe states with tensions but without net forces and thus correspond to a SSS [44]. The numbers of zero modes $n_0(\boldsymbol{k})$ and SSSs $n_s(\boldsymbol{k})$ at each $\boldsymbol{k}$ are related by the generalized Calladine-Maxwell index theorem [34,44]

$$\nu(\boldsymbol{k}) \equiv n_0(\boldsymbol{k}) - n_s(\boldsymbol{k}) = dn - n_B. \tag{1}$$

In particular, for Maxwell lattices SSSs and zero modes are created only in conjunction with one another, so that the only SSSs in a gapped Maxwell lattice are those associated with the $d$ translational modes. A Weyl point by definition is a wave vector $\boldsymbol{k}_w$ at which there is a zero mode, and there is necessarily a SSS that goes with it under PBCs. The lines of zero modes occurring along the special lines in the phase diagram also have associated lines of self-stress in real space.

We now turn to the zero modes on free surfaces. Cutting a lattice under PBCs along a lattice plane indexed by a reciprocal lattice vector $\boldsymbol{G}$ creates a finite-width strip with two free surfaces aligned along the "parallel" direction perpendicular to $\boldsymbol{G}$. In this case, it is convenient to express $\boldsymbol{k} \equiv (q, p)$ in terms of its components $q$ and $p$ parallel and perpendicular to the cut, respectively. The cut removes $\Delta n_B$ bonds and $\Delta n$ sites for each unit cell along its length or equivalently for each wave number $-\pi/a_\parallel < q < \pi/a_\parallel$ along the cut, where $a_\parallel$ is the length of the surface cell on the cut. The index theorem relating the total number of zero modes $n_0(q, \boldsymbol{G})$ (counting zero bulk modes at different $p$) to the total number of SSSs $n_s(q, \boldsymbol{G})$ at each $q$ is

$$n_0(q, \boldsymbol{G}) - n_s(q, \boldsymbol{G}) = \Delta n_B - d\Delta n. \tag{2}$$

Bulk modes in the spectrum are described by the same $\mathbf{C}(\boldsymbol{k})$ as the uncut sample but with a different set of quantized wave numbers $p$ parallel to $\boldsymbol{G}$. If a bulk mode is gapped in the periodic spectrum, it remains gapped in the strip without an associated state of self-stress. Thus, if the bulk modes are gapped at a given $q$ under PBCs, their contribution to the left-hand side of Eq. (2) will be zero, implying that only surface zero modes contribute to Eq. (2). In addition, cutting the sample will not introduce additional SSSs. The result is that Eq. (2) becomes an equation for the total number of zero surface modes on both surfaces, $n_0^{\mathrm{ST}}(q, \boldsymbol{G})$. This is a global relation that applies to every $q$ in the surface BZ at which the bulk spectrum is gapped.

As shown in Fig. 2(a), there are multiple ways to define the unit cell, corresponding to different gauges. The natural choice in the bulk is a symmetrical cell, but it is possible to obtain the number of zero modes on an edge perpendicular to $\boldsymbol{G}$ directly by selecting a compatibility matrix $\mathbf{C}(\boldsymbol{k}, \boldsymbol{G}) \equiv \mathbf{C}(q, p, \boldsymbol{G})$ in which no bonds cross the edge. As discussed in Ref. [34] and the Supplemental Material [42], $\mathbf{C}(q, p, \boldsymbol{G})$'s only $p$-dependent components are proportionate to the complex number $z = e^{i2\pi p/G}$, which is invariant under $p \to p + G$, and not to $z^{-1} = e^{-i2\pi p/G}$. Thus, $\det \mathbf{C}(q, p, \boldsymbol{G})$ has no poles within the unit circle and, by the Cauchy argument principle, its winding number around the circle $|z| = 1$ simply counts the number of its zeros with $|z| < 1$. In contrast, $\det \tilde{\mathbf{C}}(q, p, \boldsymbol{G})$ depends on $z^{-1}$ as well, and it has both poles and zeros within the circle $|z| = 1$, which are counted with opposite signs in the Cauchy integral. A zero of $\det \mathbf{C}(q, p, \boldsymbol{G})$ corresponds to

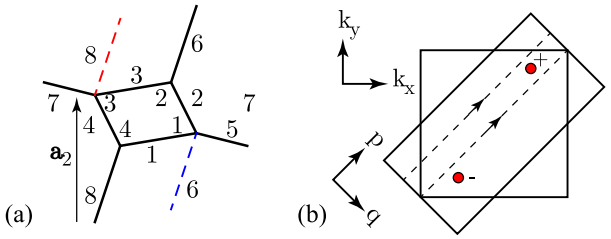


FIG. 2. (a) Different versions of the unit cell with four sites 1–4 labeled in italic script. The cell consisting of bonds, labeled 1–8 in roman script and drawn in full black, is the symmetric unit cell. A unit cell associated with a lower (upper) surface parallel to the $x$ axis is constructed by moving bond 8 through $\boldsymbol{a}_2$ (bond 6 through $-\boldsymbol{a}_2$) to the dashed red (blue) line to yield $\boldsymbol{R}_L = -\boldsymbol{a}_2$ ($\boldsymbol{R}_L = \boldsymbol{a}_2$). Panel (b) depicts the standard square BZ with two Weyl points and the BZ dual to a surface-compatible unit cell oriented at 45°. The component of $\boldsymbol{k}$ along the surface is $q$ and that parallel to $\boldsymbol{G}$ is $p$. It also shows two dashed paths, one on each side of the projected position $q_w^+$, and the "+" Weyl point at $\boldsymbol{k}_w^+$.

a surface state with a complex inverse penetration depth $\kappa = -\ln z$ with a positive real part indicating decay away from the surface into the bulk. Thus, the number of surface zero modes at $q$ is

$$\begin{aligned} n_0^S(q, \boldsymbol{G}) &= \frac{1}{2\pi i} \oint \frac{d \ln \det \mathbf{C}(q, z, \boldsymbol{G})}{dz} \\ &= -\boldsymbol{G} \cdot \boldsymbol{R}_L/(2\pi) + \tilde{n}_0^S(q, \boldsymbol{G}), \end{aligned} \tag{3}$$

where it is understood that $\boldsymbol{G}$ is the inward normal to the surface. $\boldsymbol{R}_L = 2\sum_\sigma \Delta\boldsymbol{r}_\sigma - \sum_\beta \Delta\boldsymbol{r}_\beta$, where $\Delta\boldsymbol{r}_\sigma$ is the lattice vector displacement of site $\sigma$ and $\Delta\boldsymbol{r}_\beta$ is the displacement of bond $\beta$ that converts the symmetric cell to the surface cell, is the local polarization introduced in Ref. [16]. $\tilde{n}_0^S(q, \boldsymbol{G})$ is the Cauchy integral for the symmetric unit cell. In Weyl-free regions of the phase diagram, $\tilde{n}_0^S$ reduces to the expression $-\boldsymbol{G} \cdot \boldsymbol{R}_T/2\pi$ derived in Ref. [16].

A Weyl point at $\boldsymbol{k}_w \equiv (q_w, p_w)$ is characterized by an integer winding number

$$n_w = \frac{1}{2\pi i} \oint_C d\mathbf{l} \cdot \nabla_{\boldsymbol{k}} \ln \det \mathbf{C}, \tag{4}$$

where $C$ is a contour enclosing $\boldsymbol{k}_w$. As a result, both $n_0^S(q, \boldsymbol{G})$ and $\tilde{n}_0^S(q, \boldsymbol{G})$ change each time $q$ passes through the projected position of a Weyl point. Consider a lattice with a positive (+1) Weyl point at $\boldsymbol{k}_w^+$ and a negative (−1) Weyl point at $\boldsymbol{k}_w^- = -\boldsymbol{k}_w^+$, and consider a surface with an inner normal $\boldsymbol{G}$ as depicted in Fig. 2(b) for $\boldsymbol{G} = (2\pi/a)(1, 1)$. The number of zero modes at $q$ is calculated from a contour from $p = 0$ to $p = G$ at position $q$. Choose $q^{1\pm} < q_w^\pm$ and $q^{2\pm} > q_w^\pm$. Because the two paths enclose a Weyl point, the zero-mode numbers on the two sides of the Weyl point differ by the Weyl winding number:

$$n_0^S(q^{2\pm}, \boldsymbol{G}) - n_0^S(q^{1\pm}, \boldsymbol{G}) = n_w = \pm 1. \quad (5)$$

Thus, if $n_0^S(q < q_w^+, \boldsymbol{G}) = n_1^S$, the number of zero modes for $q_w^+ < q < q_w^-$ is $n_1^S + 1$, and the number for $q > q_w^-$ is again $n_1^S$. If the total number of zero surface modes at $q$ on both surfaces is $n_0^{\mathrm{ST}}(q, \boldsymbol{G})$, the number of zero modes on the opposite surface is $n_0^{\mathrm{ST}}(q, \boldsymbol{G}) - n_1^S$ for $q < q_w^+$, $n_0^{\mathrm{ST}}(q, \boldsymbol{G}) - n_1^S - 1$ for $q_w^+ < q < q_w^-$, and back to $n_0^{\mathrm{ST}}(q, \boldsymbol{G}) - n_1^S$ for $q > q_w^1$. Figure 3 depicts the real part $\kappa$ of the inverse penetration lengths of the surface modes with and without Weyl points. The lengths diverge at the Weyl wave numbers: the surface mode turns into a bulk mode that traverses the sample.

Domain walls separating two semi-infinite lattices, which we will refer to as the upper and lower lattices as in Fig. 4, with different topological and Weyl characteristics harbor topologically protected zero modes. As in non-Weyl domain walls [16], the index describing the zero mode and SSS count on the wall is governed by the mode counts of the two domains

$$\nu^D(q, \boldsymbol{G}) = \tilde{n}_{0,L}^S(q, \boldsymbol{G}) + \tilde{n}_{0,U}^S(q, -\boldsymbol{G}), \quad (6)$$

which now changes across the Weyl wave numbers 4. This result, derived and discussed in detail in the Supplemental Material [42], describes walls with zero modes, self-stresses, or both (at different wave numbers).

The long-wavelength elasticity of central-force lattices is determined by the $\boldsymbol{k} = 0$ SSSs [34]. In the lattices we are considering, there are only two $\boldsymbol{k} = 0$ SSSs, implying that there are only two positive definite eigenvalues of the Voigt elastic matrix [45]. There are three independent strains $\boldsymbol{\varepsilon} = (\varepsilon_{xx}, \varepsilon_{yy}, \varepsilon_{xy})$, and the Voigt elastic matrix must have three positive eigenvalues and associated eigenvectors. Thus, there must be one macroscopic elastic distortion with strain $\boldsymbol{\varepsilon}^G$ that costs no energy. This is the Guest mode [46] that is a feature of all periodic Maxwell lattices except those, like the kagome lattice, with extra geometry-driven states of self-stress [34]. The long-wavelength determinant of the dynamical matrix equals zero (see the Supplemental Material [42] and Ref. [34]) when

$$\frac{k_y}{k_x} = \frac{1}{\varepsilon_{xx}^G}[\varepsilon_{xy}^G \pm \sqrt{-\det \boldsymbol{\varepsilon}^G}], \quad (7)$$

where $\det \boldsymbol{\varepsilon}^G = \varepsilon_{xx}^G \varepsilon_{yy}^G - (\varepsilon_{xy}^G)^2$ is the determinant of the Guest strain matrix. Thus, to linear order in $\boldsymbol{k}$, there are two lines in the BZ along which there is a zero mode provided $\det(\boldsymbol{\varepsilon}^G) < 0$. Either these modes are raised to finite energy by higher order terms in $\boldsymbol{k}$ not described by the elastic limit, or a single Weyl mode appears along the positive and negative parts of one of the lines. Note that this implies a quadratic rather than a linear dispersion of phonon modes near the origin and leads to inverse decay lengths that are proportional to $q^2$ rather than $q$ at long wavelengths as shown in Fig. 3.

In this work, we elucidated how Weyl modes generically arise in Maxwell frames and discussed their significance using deformed square lattices as an illustration of the more general phenomenon. Indeed, lattices with larger unit cells have additional phonon bands that more easily touch,

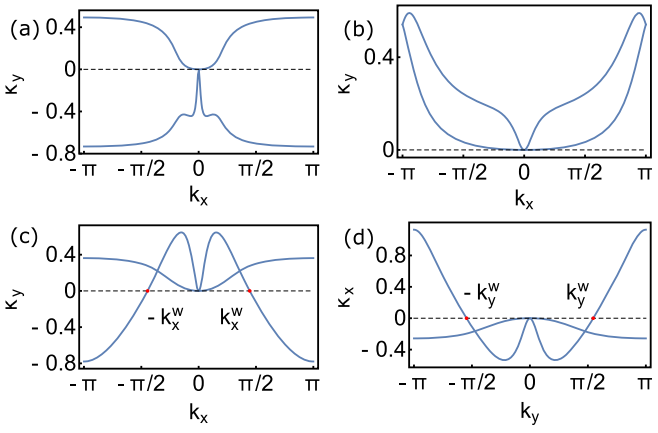


FIG. 3. Real part of the inverse penetration depths for fully gapped lattices with no Weyl points [(a) with $\boldsymbol{R}_T = (0, 0)$ and (b) with $\boldsymbol{R}_T = (0, 1)$] and (c),(d) a lattice with Weyl points. In (b), a family of zero modes has been shifted from one edge to the opposite edge relative to the unpolarized case (a), while in (c) and (d) the bulk zero modes are part of families split between two edges.

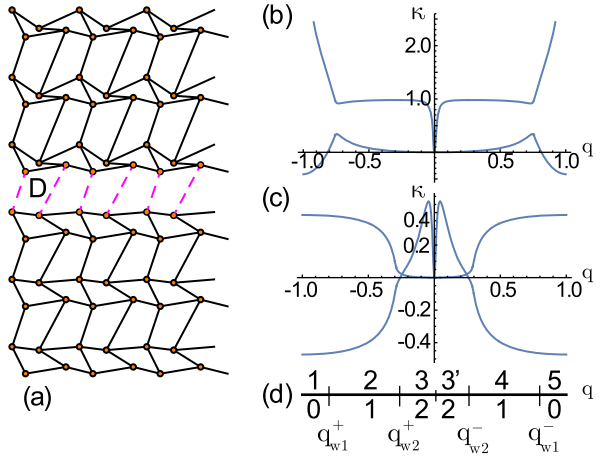


FIG. 4. (a) Two Weyl lattices with differently positioned Weyl points connected at a domain wall $D$. (b),(c) The inverse penetration depths of the free surfaces of the upper and lower lattices, respectively. The upper and lower lattices have Weyl points with respective projections onto $q$ of $q_{w1}^{\pm}$ and $q_{w2}^{\pm}$ with $|q_{w2}^+| > |q_{w1}^+|$. The free lower (upper) lattice has two zero modes penetrating downward (upward) for $q_{w1}^+ < q < q_{w1}^-$ ($q_{w2}^+ < q < q_{w2}^-$) and one for $|q| > |q_{w1}^+|$ ($|q| > |q_{w2}^+|$). Panel (d) shows how the two sets of Weyl points divide the surface BZ into five regions with 0, 1, 2, 1, and 0 zero modes in the domain wall. The existence of bulk zero modes at $\boldsymbol{k} = 0$ divides the central region with two zero modes per $q$ into two regions.

generically leading to Weyl points and even multiple pairs thereof (see the Supplemental Material [42]). Thus, our conclusions can be readily extended to other Maxwell lattices like origami metamaterials [21], random spring networks and jammed sphere packings [47], and 3D distorted pyrochlore [48] and stacked kagome lattices [18] that fulfill the Maxwell condition. We also expect the presence of Weyl modes to impact the nonlinear response (e.g., buckling) in the bulk as demonstrated for edge modes [18,19].

We are grateful to Charles Kane for many informative discussions and suggestions. D. Z. R. thanks NWO and the Delta Institute of Theoretical Physics for supporting his stay at the Institute Lorentz. M. F. was supported by the Department of Defense through the National Defense Science & Engineering Graduate Fellowship (NDSEG) Program. This work was supported in part by DMR-1104707 and DMR-1120901 (T. C. L.), as well as FOM and NWO (B. G. C., V. V.).

*Corresponding author.
drocklin@umich.edu
†Present address: Department of Physics, University of Massachusetts, Amherst, Massachusetts 01002, USA.

[1] N. Nakamura, *Geometry, Topology and Physics*, 2nd ed. (Institute of Physics Publishing, Bristol, 2008), p. 79 and Chap. 12.
[2] G. E. Volovik, *The Universe in a Helium Droplet* (Clarenden, Oxford, 2003).
[3] G. E. Volovik, Quantum analogues: From phase transitions to black holes and cosmology, in *Quantum Phase Transitions from Topology in Momentum Space Lecture Notes in Physics* Vol. 718 (Springer, Berlin, 2007), pp. 31–73.
[4] W. P. Su, J. R. Schrieffer, and A. J. Heeger, Phys. Rev. Lett. **42**, 1698 (1979).
[5] R. Jackiw and C. Rebbi, Phys. Rev. D **13**, 3398 (1976).
[6] B. I. Halperin, Phys. Rev. B **25**, 2185 (1982).
[7] F. D. M. Haldane, Phys. Rev. Lett. **61**, 2015 (1988).
[8] C. L. Kane and E. J. Mele, Phys. Rev. Lett. **95**, 146802 (2005).
[9] B. A. Bernevig, T. L. Hughes, and S.-C. Zhang, Science **314**, 1757 (2006).
[10] J. E. Moore and L. Balents, Phys. Rev. B **75**, 121306 (2007).
[11] L. Fu, C. L. Kane, and E. J. Mele, Phys. Rev. Lett. **98**, 106803 (2007).
[12] Z. Hasan and C. Kane, Rev. Mod. Phys. **82**, 3045 (2010).
[13] X.-L. Qi and S.-C. Zhang, Rev. Mod. Phys. **83**, 1057 (2011).
[14] E. Prodan and C. Prodan, Phys. Rev. Lett. **103**, 248101 (2009).
[15] M. J. Lawler, New J. Phys. **15**, 043043 (2013).
[16] C. Kane and T. C. Lubensky, Nat. Phys. **10**, 39 (2014).
[17] J. Paulose, B. G. Chen, and V. Vitelli, Nat. Phys. **11**, 153 (2015).
[18] J. Paulose, A. S. Meeussen, and V. Vitelli, Proc. Natl. Acad. Sci. U.S.A. **112**, 7639 (2015).
[19] B. G. Chen, N. Upadhyaya, and V. Vitelli, Proc. Natl. Acad. Sci. U.S.A. **111**, 13004 (2014).
[20] V. Vitelli, N. Upadhyaya, and B. G. Chen, arXiv:1407.2890.
[21] B. G. Chen, B. Liu, A. A. Evans, J. Paulose, I. Cohen, V. Vitelli, and C. D. Santangelo, arXiv:1508.00795.
[22] M. Xiao, G. Ma, Z. Yang, P. Sheng, Z. Q. Zhang, and C. T. Chan, Nat. Phys. **11**, 240 (2015).
[23] H. C. Po, Y. Bahri, and A. Vishwanath, arXiv:1410.1320.
[24] Z. Yang, F. Gao, X. Shi, X. Lin, Z. Gao, Y. Chong, and B. Zhang, Phys. Rev. Lett. **114**, 114301 (2015).
[25] L. M. Nash, D. Kleckner, V. Vitelli, A. M. Turner, and W. T. M. Irvine, Proc. Natl. Acad. Sci. U.S.A. **112**, 14495 (2015).
[26] P. Wang, L. Lu, and K. Bertoldi, Phys. Rev. Lett. **115**, 104302 (2015).
[27] Y.-T. Wang, P.-G. Luan, and S. Zhang, New J. Phys. **17**, 073031 (2015).
[28] R. Susstrunk and S. D. Huber, Science **349**, 47 (2015).
[29] T. Kariyado and Y. Hatsugai, Sci. Rep. **5**, 18107 (2015).
[30] V. Peano, C. Brendel, M. Schmidt, and F. Marquardt, Phys. Rev. X **5**, 031011 (2015).
[31] S. H. Mousavi, A. B. Khanikaev, and Z. Wang, arXiv:1507.03002.
[32] A. B. Khanikaev, R. Fleury, S. H. Mousavi, and A. Al, Nat. Commun. **6**, 8260 (2015).
[33] D. Z. Rocklin, S. Zhou, K. Sun, and X. Mao, arXiv:1510.06389.
[34] T. C. Lubensky, C. L. Kane, X. Mao, A. Souslov, and K. Sun, Rep. Prog. Phys. **78**, 073901 (2015).
[35] X. G. Wan, A. M. Turner, A. Vishwanath, and S. Y. Savrasov, Phys. Rev. B **83**, 205101 (2011).
[36] A. A. Burkov and L. Balents, Phys. Rev. Lett. **107**, 127205 (2011).
[37] A. A. Burkov, M. D. Hook, and L. Balents, Phys. Rev. B **84**, 235126 (2011).
[38] J. P. Liu and D. Vanderbilt, Phys. Rev. B **90**, 155316 (2014).
[39] S.-Y. Xu *et al.*, Science **349**, 613 (2015).
[40] L. Lu, L. Fu, J. D. Joannopoulos, and M. Soljacic, Nat. Photonics **7**, 294 (2013).
[41] L. Lu, Z. Wang, D. Ye, L. Rain, J. D. Joannopoulos, and M. Soljacic, arXiv:1502.03438v1.
[42] See Supplemental Material at http://link.aps.org/supplemental/10.1103/PhysRevLett.116.135503 for details of calculations for topological polarization and Weyl character of mechanical frames.
[43] K. Sun, A. Souslov, X. Mao, and T. C. Lubensky,, Proc. Natl. Acad. Sci. U.S.A. **109**, 12369 (2012).
[44] C. R. Calladine, Int. J. Solids Struct. **14**, 161 (1978).
[45] N. W. Ashcroft and N. D. Mermin, *Solid State Physics*, 1st ed. ( Thomson Learning Inc, New York, 1976).
[46] S. D. Guest and J. W. Hutchinson, J. Mech. Phys. Solids **51**, 383 (2003).
[47] D. M. Sussman, O. Stenull, and T. C. Lubensky, arXiv:1512.04480.
[48] O. Stenull, C. L. Kane, and T. C. Lubensky (unpublished).